5-1-2015

Structural and functional MRI abnormalities of cerebellar cortex and nuclei in SCA3, SCA6 and Friedreich's ataxia

Maria R. Stefanescu
Universitätsklinikum Essen

Moritz Dohnalek
Universitätsklinikum Essen

Stefan Maderwald
Universität Duisburg-Essen

Markus Thürling
Universitätsklinikum Essen

Martina Minnerop
Forschungszentrum Jülich (FZJ)

See next page for additional authors

doi:10.1093/brain/awv064 BRAIN 2015: 138; 1182–1197 | 1182

BRAIN
A JOURNAL OF NEUROLOGY

Structural and functional MRI abnormalities of cerebellar cortex and nuclei in SCA3, SCA6 and Friedreich's ataxia

Maria R. Stefanescu,[1,2] Moritz Dohnalek,[1] Stefan Maderwald,[2] Markus Thürling,[1,2] Martina Minnerop,[3,4] Andreas Beck,[5] Marc Schlamann,[6] Joern Diedrichsen,[7] Mark E. Ladd[2,6,8] and Dagmar Timmann[1]

Spinocerebellar ataxia type 3, spinocerebellar ataxia type 6 and Friedreich's ataxia are common hereditary ataxias. Different patterns of atrophy of the cerebellar cortex are well known. Data on cerebellar nuclei are sparse. Whereas cerebellar nuclei have long been thought to be preserved in spinocerebellar ataxia type 6, histology shows marked atrophy of the nuclei in Friedreich's ataxia and spinocerebellar ataxia type 3. In the present study susceptibility weighted imaging was used to assess atrophy of the cerebellar nuclei in patients with spinocerebellar ataxia type 6 ($n = 12$, age range 41–76 years, five female), Friedreich's ataxia ($n = 12$, age range 21–55 years, seven female), spinocerebellar ataxia type 3 ($n = 10$, age range 34–67 years, three female), and age- and gender-matched controls (total $n = 23$, age range 22–75 years, 10 female). T_1-weighted magnetic resonance images were used to calculate the volume of the cerebellum. In addition, ultra-high field functional magnetic resonance imaging was performed with optimized normalization methods to assess function of the cerebellar cortex and nuclei during simple hand movements. As expected, the volume of the cerebellum was markedly reduced in spinocerebellar ataxia type 6, preserved in Friedreich's ataxia, and mildy reduced in spinocerebellar ataxia type 3. The volume of the cerebellar nuclei was reduced in the three patient groups compared to matched controls (P-values < 0.05; two-sample t-tests). Atrophy of the cerebellar nuclei was most pronounced in spinocerebellar ataxia type 6. On a functional level, hand-movement-related cerebellar activation was altered in all three disorders. Within the cerebellar cortex, functional magnetic resonance imaging signal was significantly reduced in spinocerebellar ataxia type 6 and Friedreich's ataxia compared to matched controls (P-values < 0.001, bootstrap-corrected cluster-size threshold; two-sample t-tests). The difference missed significance in spinocerebellar ataxia type 3. Within the cerebellar nuclei, reductions were significant when comparing spinocerebellar ataxia type 6 and Friedreich's ataxia to matched controls ($P < 0.01$, bootstrap-corrected cluster-size threshold; two-sample t-tests). Susceptibility weighted imaging allowed depiction of atrophy of the cerebellar nuclei in patients with Friedreich's ataxia and spinocerebellar ataxia type 3. In spinocerebellar ataxia type 6, pathology was not restricted to the cerebellar cortex but also involved the cerebellar nuclei. Functional magnetic resonance imaging data, on the other hand, revealed that pathology in Friedreich's ataxia and spinocerebellar ataxia type 3 is not restricted to the cerebellar nuclei. There was functional involvement of the cerebellar cortex despite no or little structural changes.

1 Department of Neurology, University of Duisburg-Essen, Essen, Germany
2 Erwin L. Hahn Institute for Magnetic Resonance Imaging, University of Duisburg-Essen, Essen, Germany
3 Institute of Neuroscience and Medicine (INM-1), Research Centre Jülich, Jülich, Germany
4 Department of Neurology, University of Bonn, Bonn, Germany
5 Department of Computer Sciences, University of Düsseldorf, Düsseldorf, Germany
6 Department of Diagnostic and Interventional Radiology and Neuroradiology, University of Duisburg-Essen, Essen, Germany
7 Institute of Cognitive Neuroscience, University College London, London, UK
8 Division of Medical Physics in Radiology, University of Heidelberg and German Cancer Research Centre, Heidelberg, Germany

Received September 17, 2014. Revised January 2, 2015. Accepted January 21, 2015. Advance Access publication March 28, 2015

Correspondence to: Maria Roxana Stefanescu,
Department of Neurology, University Clinic Essen,
University of Duisburg-Essen,
Hufelandstrasse 55,
45147 Essen,
Germany
E-mail: stefanescu.m.roxana@gmail.com

Keywords: hereditary ataxia; dentate nuclei; spinocerebellar degeneration; structural magnetic resonance imaging; functional magnetic resonance imaging; cerebellar atrophy

Abbreviations: EPI = echoplanar imaging; MPRAGE = magnetization prepared rapid acquisition gradient echo; SARA = Scale for the Assessment and Rating of Ataxia; SCA = spinocerebellar ataxia; SUIT = spatially unbiased atlas template of the cerebellum and brainstem; SWI = susceptibility-weighted imaging; TCIV = total intracranial volume

Introduction

Hereditary ataxias are slowly progressive degenerative disorders that affect the cerebellum and cerebellar pathways to various degrees (Schulz *et al.*, 2009; Dürr *et al.*, 2010; Klockgether, 2011). Key symptoms are motor incoordination and disordered balance, and manifest as limb ataxia, ataxia of stance and gait, dysarthria, and oculomotor signs. Extracerebellar involvement is frequent. Friedreich's ataxia is the most common recessive ataxia in Europe and the USA. Spinocerebellar ataxias type 3 and 6 (SCA3, SCA6) are among the most common autosomal dominant ataxias (van de Warrenburg *et al.*, 2014). Although cerebellar dysfunction is the main cause of ataxia in SCA6, sensory dysfunction plays the most important role in Friedreich's ataxia and contributes to ataxia in SCA3 to varying extent.

The cerebellum, however, is involved in all three hereditary ataxias (Seidel *et al.*, 2012; Koeppen *et al.*, 2013). Histological studies of post-mortem cerebellar tissue show clear differences between SCA6 on the one hand and Friedreich's ataxia and SCA3 on the other. There is marked reduction of the cerebellar cortex in SCA6 with predominant loss of Purkinje cells, whereas the cerebellar cortex is largely preserved in Friedreich's ataxia and SCA3 (Sasaki *et al.*, 1998; Koeppen, 2005; Scherzed *et al.*, 2012; Koeppen and Mazurkiewicz, 2013). On the level of the cerebellar nuclei, the opposite appears to be the case. The size of the cerebellar nuclei is reduced in Friedreich's ataxia and SCA3. In both disorders, cerebellar nuclei show the same pattern of 'grumose' degeneration (Koeppen *et al.*, 2007; Koeppen and Mazurkiewicz, 2013). The cerebellar nuclei are generally considered preserved in SCA6, although newer studies show some involvement of the cerebellar nuclei (Gierga *et al.*, 2009; Wang *et al.*, 2010). In all three disorders the inferior olive is largely preserved (Koeppen, 2005, 2013).

The differences in pathology within the cerebellar cortex can be readily observed in diagnostic brain scans. Whereas marked cerebellar atrophy and reduction of grey matter volume is a hallmark of SCA6, cerebellar atrophy is uncommon in Friedreich's ataxia and comparatively mild in SCA3 at least in the early stages of the disease (Klockgether *et al.*, 1991; Bürk *et al.*, 1996; Schulz *et al.*, 2010). As yet, assessment of accompanying atrophy of the cerebellar nuclei is not part of the diagnostic routine. This may change in the future. Susceptibility-weighted imaging (SWI) is now routinely used to show small bleedings and venous abnormalities (Gasparotti *et al.*, 2011). The iron content in the cerebellar nuclei is high, and SWI allows visualization of the cerebellar nuclei and quantification of their volume in healthy subjects (Diedrichsen *et al.*, 2011; Maderwald *et al.*, 2012). As yet, application of SWI has not been systematically assessed to diagnose and quantify accompanying atrophy of the cerebellar nuclei in hereditary ataxias.

The mere size of the cerebellar cortex and nuclei, however, does not necessarily reflect function. Little is known about the remaining function and possible compensatory mechanisms within the cerebellar cortex and nuclei in hereditary ataxias. Here, functional MRI studies can be of help. Until recently, activations of the cerebellar nuclei were difficult to obtain because of their small size and high iron content (Habas, 2010). The introduction of ultra-high-field MRI and the development of optimized region of interest-based normalization methods have made reliable functional MRI studies at the level of the dentate nuclei possible (Diedrichsen *et al.*, 2011; Küper *et al.*, 2012).

In the present study, SWI was used to show atrophy of cerebellar nuclei in SCA6, Friedreich's ataxia and SCA3. We tested the hypothesis that cerebellar nuclei are smaller in Friedreich's ataxia and SCA3 compared to healthy controls, but relatively preserved in SCA6. Functional MRI (7 T) of a simple hand movement was used to assess function of the cerebellar cortex and nuclei. Great care was taken to ensure that movement performance did not differ between groups. We predicted that functional MRI signal would be decreased in the cerebellar cortex in SCA6, but relatively preserved or compensatorily increased in Friedreich's ataxia and SCA3 compared to controls. On the level of the nuclei we expected a reduced signal in

SCA3 and Friedreich's ataxia, and a preserved or compensatorily increased functional MRI signal in the patients with SCA6. The results are discussed in the light of histopathological data and current knowledge of the underlying physiology of the functional MRI signal in the cerebellum.

Materials and methods

Subjects

A total of 34 patients [15 female, 19 male; mean age 48.06 years, standard deviation (SD) 14.07 years, range 21–76] and 23 neurologically healthy subjects (10 female, 13 male; mean age 46.39, SD 15.82 years, 22–75 years) were included. The SCA6 group consisted of 12 patients (five female, seven male; mean age 57.75, SD 12.06 years, range 41–76), the Friedreich's ataxia group consisted of 12 patients (seven female, five male; mean age 39.08, SD 12.87 years, range 21–55), and the SCA3 group of 10 patients (three female, seven male; mean age 47.20, SD 10.58 years, range 34–67). An additional two patients were excluded because of motion artefacts, another four patients because of claustrophobia. Age- and gender-matched subgroups of controls were selected for direct comparison with individual patient groups (SCA6 controls: five female, seven male; mean age 57.08, SD 12.3, range 34–75; Friedreich's ataxia controls: seven female, five male; mean age 39.92, SD 13.19 years, range 22–59; SCA3 controls: three female, seven male; mean age 46.60, SD 10.80 years, range 34–67).

All patients had genetically proven disease. Clinical ataxia scores were assessed based on the Scale for the Assessment and Rating of Ataxia (SARA; Schmitz-Hübsch *et al.*, 2006) by an experienced neurologist (D.T.) on the MRI scanning day. Clinical data are summarized in Supplementary Table 1. Two patients with Friedreich's ataxia and two corresponding control group subjects were left-handed based on the Edinburgh Handedness Questionnaire (Oldfield, 1971). All other participants were right-handed. The study was approved by the local ethics committee. All subjects gave informed oral and written consent.

MRI scanning

Structural and functional images were acquired using a 7 T whole-body MRI scanner (Siemens Healthcare) with a single-channel transmit (Tx) and 32 channel receive (Rx) head coil (Nova Medical Head Coil 1Tx / 32Rx). Heads were fixed with foamed material. A training session of the hand movement was performed before scanning and outside the scanner (for details see below). Scanning started with an anatomical image followed by a brief training session of the hand movement and finally the functional MRI session. Scanning ended with the SWI sequence. After scanning, participants completed a questionnaire grading discomfort and physiological sensations (e.g. vertigo, light flashes) on an 11-point scale during table movement and when the table was stationary (Theysohn *et al.*, 2008). Discomfort and physiological sensations were generally mild and not significantly increased in patients compared to controls (see Supplementary material for details).

Structural MRI

Magnetization prepared rapid acquisition gradient echo (MPRAGE) images were used to calculate the volume of the entire cerebellum, the volume of the cerebrum, and the total intracranial volume (TICV). Volumetric analysis was performed semi-automatically by an experienced lab technician with the help of ECCET software (http://eccet.de/). Details of the analysis have been reported previously (Brandauer *et al.*, 2008; Weier *et al.*, 2012). The MPRAGE sequence was acquired with the following parameters: repetition time = 2500 ms, echo time = 2.05 ms, inversion time = 1100 ms, GRAPPA (generalized autocalibrating partially parallel acquisition) R = 2, flip angle 7°, field of view = 256 × 176 mm^2, matrix 256 × 256, bandwidth of 210 Hz/Px, 176 slices per slab, voxel size 1 mm × 1 mm × 1 mm, acquisition time = 7.49 min.

SWI images were used to calculate the volume of the dentate nuclei. Dentate nuclei were visually identified and then marked manually as regions of interest using MRIcron software (http://www.mccauslandcenter.sc.edu/mricro/mricron) by the same lab technician. The region of interest drawing followed the corrugated wall of the dentate nucleus as well as possible. Drawings were done directly in the SWI images. Drawings were corrected based on the magnitude images because the extent of the dentate nucleus is often overestimated in SWI images due to frequency shift distributions in phase images (Maderwald *et al.*, 2012; Marques *et al.*, 2012). Cerebellar nuclei are depicted as hypointensities (Fig. 1). A 3D SWI sequence was acquired with the following parameters: repetition time = 50 ms, echo time 1 = 23.5 ms, echo time 2 = 31.2 ms, parallel MRI GRAPPA R = 4, flip angle 18°, field of view = 224 × 182 mm^2, matrix 448 × 364, bandwidth = 160 Hz/Px, 144 axial slices for covering the cerebellum, slice thickness 0.5 mm, voxel size 0.5 mm × 0.5 mm × 0.5 mm, acquisition time = 13:05 min. Dentate nuclei were drawn on the images with echo time 2 = 31.2 ms. Dentate volume is reported as the sum of the right and left nuclei.

For statistical comparisons all volumes were expressed as percentage of total intracranial volume (TICV) (% TICV = targeted volume / TICV × 100). The technician did not know whether a patient or a control subject was being analysed.

Functional MRI

Behavioural task

The right lower arm and hand rested on the right thigh. Subjects performed opening and closing movements of the right fist. Movements were paced at 1.66 Hz using both auditory and visual cues. Subjects were instructed to open the fist to one tone and close it to the next. A 2 kHz tone was used which could be clearly differentiated from the scanner noise. The tone was applied using plastic tubes and small sponge ear plugs to both ears. In addition, the background colour changed between white and red in the MRI bore using a projection screen. Subjects were able to recognize the change in colour despite instructions to keep their eyes closed during the experiment. Subjects performed one functional MRI run with alternating rest and active blocks. The movement was trained

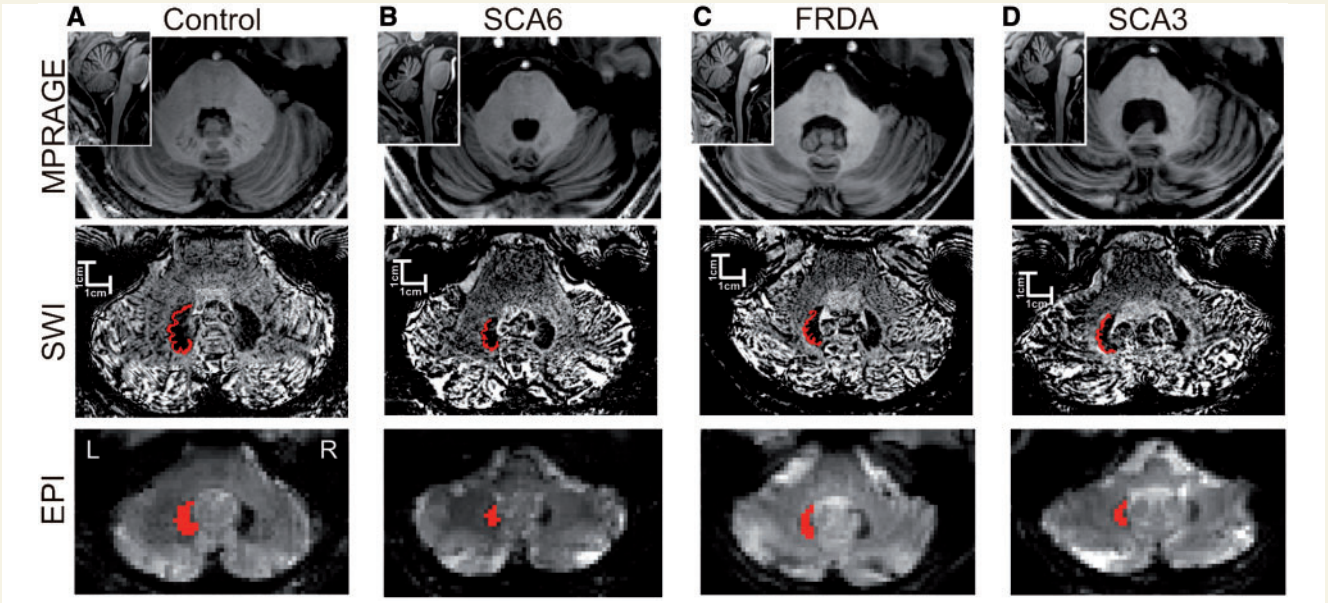

Figure 1 Characteristic structural MRI examples. (**A**) A control subject (67 years, male); (**B**) a patient with SCA6 (54 years, male); (**C**) a patient with Friedreich's ataxia (FRDA; 32 years, female); and (**D**) a patient with SCA3 (58 years, female). *Top row*: Axial slices of MPRAGE acquisition. Small insert shows sagittal images. Marked cerebellar atrophy is visible in the patient with SCA6, large fourth ventricle in the patient with SCA3, and mild atrophy of the spinal cord in the patient with Friedreich's ataxia. *Second row*: Axial slices of SWI acquisition of the same subjects. Dentate nuclei are visible as hypointensities. Drawings of the dentate nuclei used for quantification of volumes are superimposed on the left (red). Dentate nuclei were smaller in the three patients. Dentate atrophy was most marked in the patient with SCA6. *Bottom row*: Axial slices of EPI acquisition. Bean-shaped drawings of the dentate nuclei used for region of interest-based normalization are superimposed on the left (red). L = left; R = right.

outside the scanner for at least 10 min. During training subjects were able to look at their hand. In the scanner, following the anatomical scan, subjects received a brief training period without scanning, which was followed by a brief training period with scanning to make sure movements were done only during active blocks and with the correct frequency. All subjects used their right hand, and there was the same number of left handers in the patient and their matched control groups.

An MRI-compatible glove (5DT-Data-Glove-14-MRI; Fifth Dimension Technologies; http://www.5dt.com) was used to monitor movements during scanning and to analyse performance off-line. Finger flexion was measured based on fibre optic sensors (two sensors per finger; sampling rate 100 Hz). In case subjects missed active blocks or moved during rest blocks, scanning sessions were interrupted and repeated. Glove data were processed with self-written software in MATLAB®. Movement frequency and amplitude were assessed based on the distal sensor of the middle finger. Analyses of variance with repeated measures were used to compare between groups and blocks (PASW Statistics 18, formerly SPSS).

Functional MRI data acquisition

Subjects performed nine rest blocks and eight active blocks. Each run started and ended with a rest block. Rest blocks included 10 scans and lasted 30.6 s, and active blocks lasted 32.4 s and included 11 scans. Functional images were acquired using a 2D echoplanar imaging (EPI) sequence: repetition time = 3000 ms, echo time = 20 ms, acquisition time = 9.26 min, fat saturation flip angle = 30°, phase partial Fourier 7/8, field of view = 220 × 220 mm^2, matrix 110 × 110, bandwidth = 1108 Hz/Px, slice thickness 2.0 mm, voxel size 2.0 mm × 2.0 mm × 2.2 mm. Parallel MRI (parallel acquisition techniques) GRAPPA with an acceleration factor R = 3 was used to reduce image distortions (Poser and Norris, 2009) which was further aided by the fast gradient mode and a raw filter. Each EPI session consisted of a total of 178 (nine rest blocks × 10 scans, eight active blocks × 11 scans) mosaic scans with 72 coronal slices. Four dummy scans were included at the beginning and one at the end of the session. The gradient shape of the EPI readout gradients was sinusoidal. Coronal orientation was used with phase encoding in the feet to head direction (Thürling *et al.*, 2011).

The Siemens Physiologic Monitoring Unit (PMU) was used to collect breathing and pulse rate synchronized to magnetic resonance scanning (www.medical.siemens.com/). Pulse oximetry was recorded using a wireless recording device clipped to the subjects' left index finger. A respiratory bellows was attached to the subject using a belt. The latter was part of the Siemens Physiological ECG and Respiratory Unit (PERU). The signals of these sensors were monitored during scanning and used off-line as regressors (see below).

7 T functional MRI data analysis

SPM8 (Wellcome Department of Cognitive Neurology, London, UK) was used to analyse the MRI data. The five dummy scans and the last scan of each of the eight active blocks were excluded. One hundred and seventy functional

scans were included in the analysis. The functional images were realigned and resliced with respect to the first volume from the first block, providing the six parameters of an affine 'rigid-body' transform and a mean image per participant. Functional MRI data were analysed with a region of interest approach. Regions of interest were the cerebellar cortex, and dentate nuclei. In addition, cerebral activations with a focus on primary motor cortex were analysed to exclude a general and therefore non-specific decrease of functional MRI signal in patients.

DARTEL normalization was used to morph the individual's entire brain into the MNI atlas space (Ashburner, 2007). Normalization of the cerebellum was performed using the SUIT v2.7 toolbox in SPM8 (www.icn.ucl.ac.uk/motorcontrol/imaging/suit.htm; Diedrichsen, 2006). RETROICOR (retrospective image-based correction) was applied to correct for physiological motion effects (Glover *et al.*, 2000). PhLEM Toolbox (https://sites.google.com/site/phlemtoolbox/) and self-written software in MATLAB® were used to prepare pulse and breathing data as regressors (Verstynen and Deshpande, 2011). The default brightness threshold (defaults.mask.thresh) in SPM was set to 0.3 to avoid exclusion of voxels in the dentate nucleus, which have very low mean signal intensity due to high iron content (Diedrichsen *et al.*, 2011; Stefanescu *et al.*, 2013). First-level statistical analysis (first general linear model, GLM; Friston *et al.*, 1995) was applied with a temporal high-pass filter (cut-off 128 s) to remove slowly varying trends.

One sample *t*-tests (active blocks > rest blocks) were performed for each group (SCA6, Friedreich's ataxia, SCA3, SCA6 controls, Friedreich's ataxia controls, SCA3 controls). Paired sample *t*-tests (controls > patients; patients > controls) were performed to compare between patient groups and their matched controls. Age and movement frequency were used as covariates of no interest. Height threshold was set as $P < 0.001$ regarding the cerebrum, primary motor cortex and cerebellar cortex, and $P < 0.01$ regarding the cerebellar nuclei. Bootstrapping was used to correct for multiple comparisons (Hayasaka and Nichols, 2003). Sets of group samples were selected from contrast images, and each independently multiplied with 1 or −1 to randomize the sign. For each of these fake data sets, a t-map was calculated and the t-value was determined at the uncorrected threshold $P < 0.001$ (cerebrum, primary motor and cerebellar cortex) and $P < 0.01$ (cerebellar nuclei). Repeating this process 10 000 times, threshold values that would only occur in 5% of the random data sets were determined. The minimal cluster size was obtained for both the patient and control groups. In case the cluster size criterion was fulfilled, activation was regarded as significant.

Normalization of cerebral cortex

Functional data were normalized to the DARTEL anatomical template (colin27T1_seg.nii) with 1.5 mm^3 isotropic resolution that matched the anatomical image. After smoothing the normalized data with a Gaussian filter of 8 mm full-width at half-maximum, the first statistical step was applied with the physiological data correction as nuisance regressors for each individual participant. The cerebrum (excluding the cerebellum) of the DARTEL anatomical template was used as explicit mask. Region of interest of the primary motor cortex was defined based on the SPM Anatomy toolbox v2.0 (Eickhoff *et al.*, 2005). Small volume correction was performed (Geyer *et al.*, 1996).

Normalization of cerebellar cortex

For the normalization of the cerebellar cortical data, the T_1-weighted images were deformed to fit the spatially unbiased atlas template (SUIT) of the human cerebellum using the SUIT toolbox (version 2.7) in SPM8 (http://www.icn.ucl.ac.uk/motorcontrol/imaging/suit.htm; Diedrichsen, 2006). Initially the program isolates the cerebellum and creates a mask. These masks were manually corrected with the help of MRIcron software (http://www.mccauslandcenter.sc.edu/mricro/mricron/). SUIT toolbox version 2.7 uses the DARTEL-algorithm for normalization (Ashburner, 2009), which deforms the cerebellum to simultaneously fit the probability maps or cortical grey matter, white matter and deep cerebellar nuclei to an atlas template. This non-linear deformation was then applied to each contrast image from the individual participants. The normalized images were then smoothed by a 3D convolution with an isotropic Gaussian kernel of 6 mm full-width at half-maximum. Small volume correction was performed based on the probabilistic atlas of the cerebellar cortex (Diedrichsen *et al.*, 2009).

Normalization of dentate nuclei

Region of interest-based SUIT normalization was used to normalize the dentate nuclei (Diedrichsen *et al.*, 2011). Dentate nuclei were visually identified as hypointensities in the realigned echoplanar images (Fig. 1). Bean-shaped dentate nuclei were traced manually as rough 'hull' regions of interest using MRIcron (http://www.mccauslandcenter.sc.edu/mricro/mricron/). It cannot be fully ruled out that 'hull' regions of interest included parts of the interposed nuclei because a clear separation between the dorsorostral dentate and interposed nuclei was frequently not possible in the EPI scans. In addition to SUIT DARTEL normalization, region of interest-based SUIT normalization attempts to simultaneously match the T_1-weighted image of the individual to the high-resolution SUIT template and the individual 'hull' region of interest to a SUIT template of the dentate nuclei (Diedrichsen *et al.*, 2011). The contrast images were masked to include only dentate voxels, normalized to the most recent SUIT dentate template, spatially resampled to 1 mm × 1 mm × 1 mm, and smoothed with a Gaussian filter of 2 mm full-width at half-maximum (Diedrichsen *et al.*, 2011; Küper *et al.*, 2011). To localize the dentate activations, the dentate template was divided into four subdivisions: dorsorostral, dorsocaudal, ventrorostral, and ventrocaudal as described by Küper *et al.* (2011).

Results

Structural MRI

Figure 1 (top row) shows individual examples of MPRAGE images. Marked atrophy of the cerebellum is present in the patient with SCA6, and mild atrophy with enlargement of the fourth ventricle is seen in the patient with SCA3. In the patient with Friedreich's ataxia, the size of the cerebellum is not different compared to the control subject, but mild atrophy of the cervical cord can be observed. On a group level, cerebellar volume (% TICV) was significantly reduced

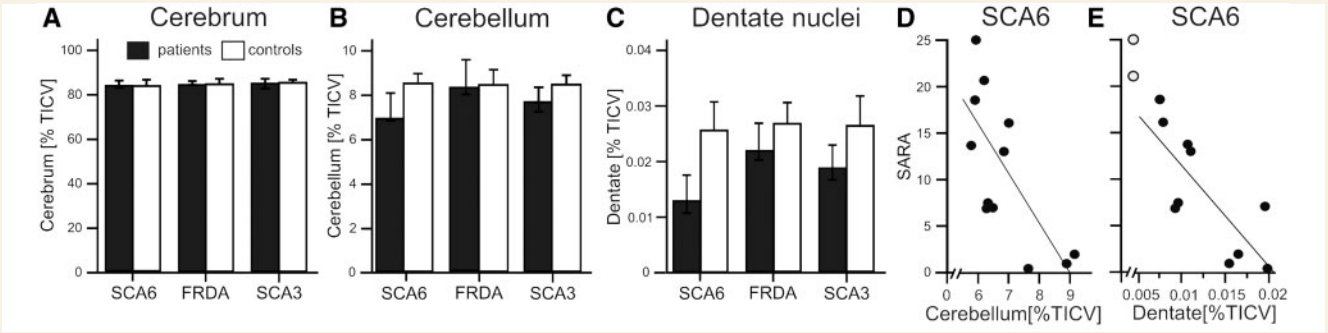

Figure 2 Volumetric analysis of cerebellum and dentate nuclei. Group mean volumes and standard deviations of (**A**) cerebrum (cerebellum excluded), (**B**) cerebellum, and (**C**) dentate nuclei (sum of right and left) in patients with SCA6, Friedreich's ataxia, and SCA3 and their matched control groups. Volumes are expressed as percentage of the total intracranial volume (% TICV). Scatter plots comparing total SARA score and volume of the cerebellum and dentate nuclei in patients with SCA6 are shown in **D** and **E**. Note negative correlations.

in patients with SCA6 compared to matched controls [T(13.91) = −4.54, $P < 0.001$; unpaired *t*-test, assuming unequal variances] and in patients with SCA3 compared to matched controls [T(18) = −3.35, $P = 0.004$] (Fig. 2B). Volume reduction was less in patients with SCA3 compared to those with SCA6. In patients with Friedreich's ataxia, cerebellar volume was not significantly different [T(22) = −0.40, $P = 0.68$]. There was no significant difference in cerebral volume expressed in % TICV comparing patient groups and their matched controls (*P*-values > 0.7) (Fig. 2A).

Figure 1 (middle row) shows SWI images of the same individuals shown in the top row. Dentate nuclei are seen as hypointensities. Dentate nuclei were smaller in the three patients compared to the control subject. Nuclei were smallest in the patient with SCA6. Likewise, on the group level, volumes of dentate nuclei (% TICV) were most markedly reduced in SCA6 patients compared to matched controls [T(20) = −5.93, $P < 0.001$; unpaired *t*-test] (Fig. 2C). In 2 of 12 patients with SCA6, dentate nuclei were not visible in the SWI images and were not included in the group mean. Dentate volumes were also smaller in Friedreich's ataxia and SCA3 patients compared to their matched controls [Friedreich's ataxia versus matched controls: T(22) = −2.73, $P = 0.012$; SCA3 versus matched controls: T(18) = −3.60, $P = 0.002$] (Fig. 2C).

There was a significant negative correlation comparing both cerebellar and dentate volumes with total SARA score in SCA6 patients (cerebellar volume: R = −0.716, $P = 0.009$; dentate volume: R = −0.780, $P = 0.008$; Pearson correlation coefficient; Fig. 2D and E). Note that the two patients with SCA6 with absent dentate nuclei (therefore not included in correlation analysis of SARA and dentate volume) had the highest SARA scores in the SCA6 group, i.e. were the most clinically affected (total SARA scores: 20.5 and 25). No significant correlations were observed in patients with SCA3 and Friedreich's ataxia (R values = −0.270–0.084, *P*-values = 0.450–0.956). The more diffuse brain pathology in Friedreich's ataxia and SCA3 compared to SCA6 may explain the lack of correlation.

No significant correlations were observed comparing trinucleotide repeat lengths and degree of atrophy of the cerebellar cortex and nuclei in any of the three groups (all *P*-values > 0.05). The best correlation coefficient was observed comparing CAG-repeat length and atrophy of the dentate nuclei in patients with SCA6 (R = −0.583, $P = 0.076$).

Functional MRI

Behavioural data

Subjects were expected to perform 27 opening and closing movements of the fist within one active block of 32.4 s. This number was very closely met by all patient groups (SCA6 = mean 26.47 SD 1.4; Friedreich's ataxia = 26.36 SD 0.81; SCA3 = 26.88 SD 0.15) and their matched controls (SCA6 controls = 26.95 SD 0.07; Friedreich's ataxia controls = 26.98 SD 0.05; SCA3 controls = 26.89 SD 0.19) (Supplementary Fig. 1A). Analysis of variance with repeated measures showed no significant differences in movement frequency between SCA6 and SCA3 patients and their matched controls [SCA6 versus controls: $F(1,22) = 1.36$, $P = 0.255$; SCA3 versus controls: $F(1,18) = 0.006$, $P = 0.938$]. The small difference between Friedreich's ataxia patients and controls was significant [$F(1,22) = 6.92$, $P = 0.015$]. There were no block effects, and no block by group interactions (all *P*-values > 0.098).

Regarding movement amplitudes, there were no significant differences between any of the patient and control groups (all *P*-values > 0.085). There were no significant block effects (all *P*-values > 0.117), and no significant block × group interactions (all *P*-values > 0.232) (Supplementary Fig. 1B).

Functional MRI data

Cerebral activations

Activation of the cerebral cortex was strongest in left primary motor cortex (Brodmann area 4; M1) in the three patient groups and their matched control groups.

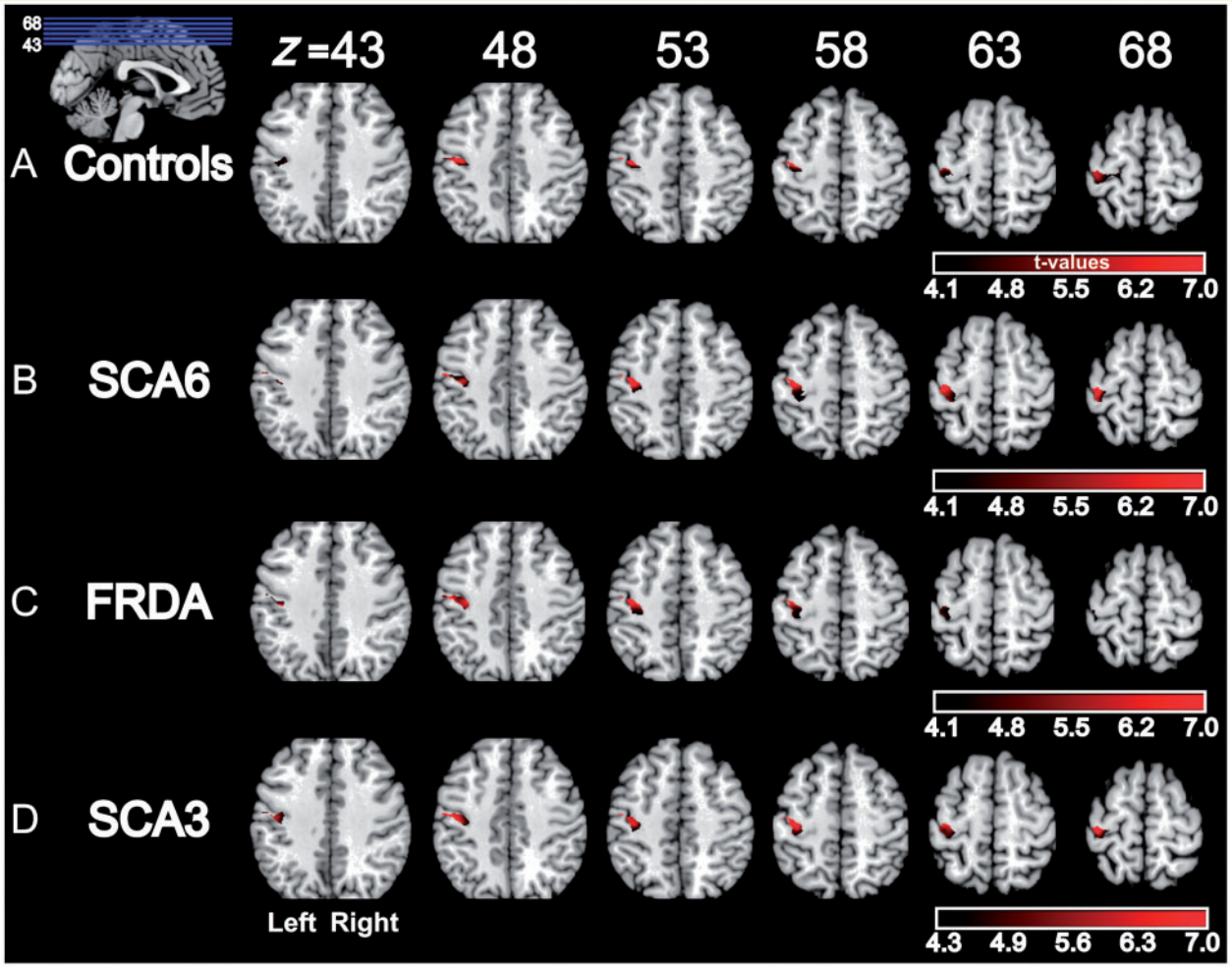

Figure 3 Functional MRI results in the left primary motor cortex. Hand movement-related activations in one of the control groups (Friedreich's ataxia controls) and in the three patient groups (SCA6, Friedreich's ataxia, SCA3) are shown in **A**–**D** (one-sample *t*-tests). Data are shown at a height threshold of $P < 0.001$ uncorrected; see Supplementary Table 2 for bootstrap-corrected cluster-size thresholds. Age and movement frequency were used as covariates of no interest. Functional MRI results are mapped onto axial sections of the colin27T1_seg template from the Anatomy toolbox v2.0 (Eickhoff *et al.*, 2005). Positions of the coronal slices are indicated in a sagittal view of the template. z = MNI coordinate.

Subtraction analysis did not reveal significant differences within left area 4 between any of the three disease groups and their matched control groups ($P < 0.001$, bootstrap-corrected cluster-size threshold; paired samples *t*-test). Activations of left area 4 are shown in Fig. 3, and local maxima and cluster sizes are summarized in Supplementary Table 2. For illustration purposes, functional MRI data are shown in only one of the matched control groups (Friedreich's ataxia controls) compared to the three patient populations throughout this article.

Considering whole brain analysis, additional activations were present in secondary motor areas as well as primary and secondary sensory areas in both patient and control groups (for details see Supplementary material, Supplementary Fig. 2 and Supplementary Table 3). Compared to their matched control groups, patients with SCA6 showed higher activations in the left anterior cingulate gyrus, and patients with Friedreich's ataxia showed higher activations in left Brodmann area 6 ($P < 0.001$, bootstrap-corrected cluster-size threshold; paired samples *t*-test). In the SCA3 group, activations were more prominent in Brodmann area 6 with additional activations of inferior frontal gyrus (Brodmann area 44) bilaterally compared to controls. In addition, activation in secondary sensory areas was more extended. However, none of these differences was significant (for details on group comparisons see Supplementary materials and Supplementary Table 4).

Cerebellar cortex

Figure 4A shows that hand movements led to strong activations within the known superior (lobules V and VI) and inferior (lobule VIII) hand representations in the cerebellar

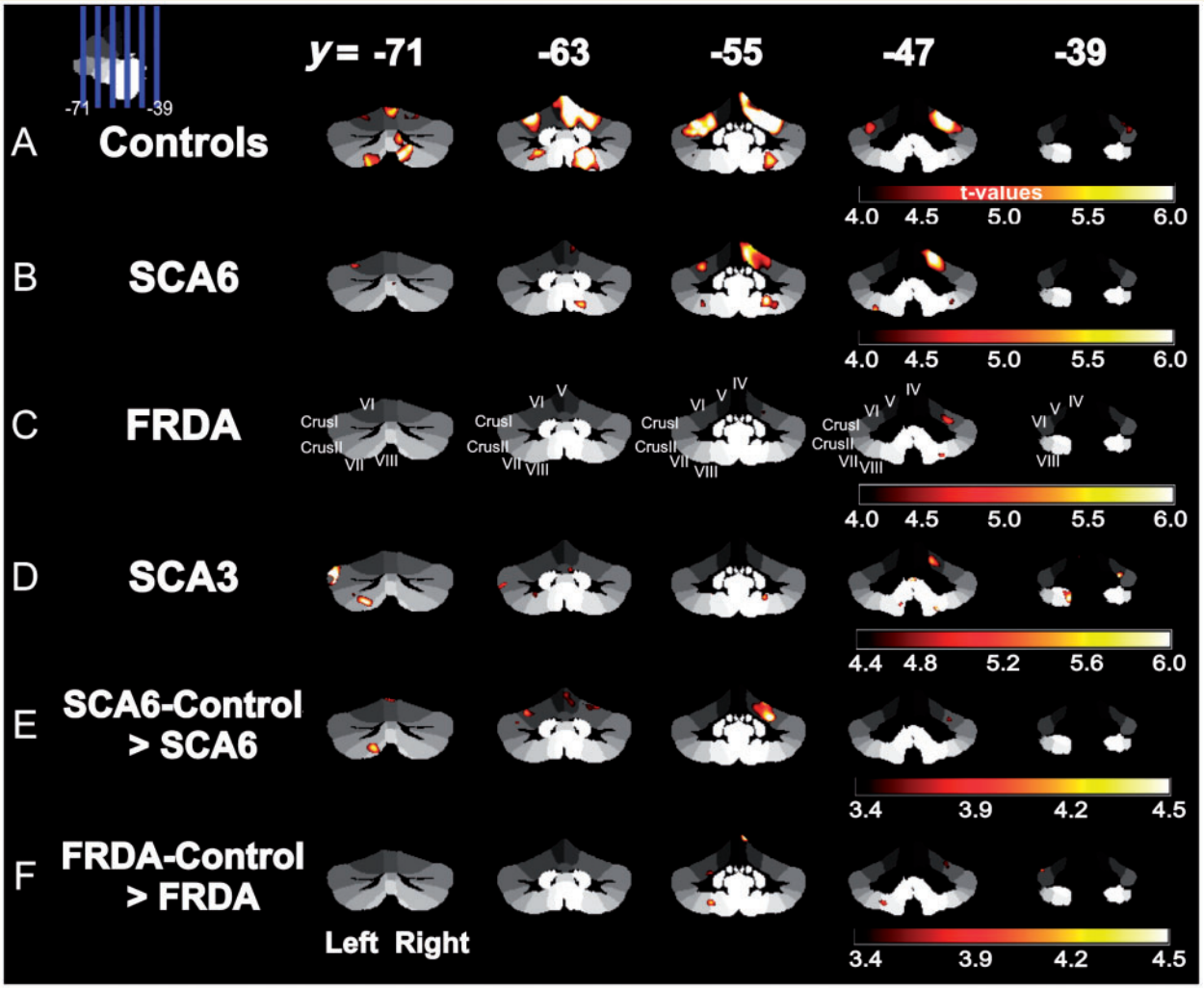

Figure 4 Functional MRI results in the cerebellar cortex. Hand-movement-related activations in one of the control groups (**A**, Friedreich's ataxia controls) and the three patient groups (**B**, SCA6; **C** Friedreich's ataxia; **D**, SCA3) are mapped onto coronal sections of the cerebellar SUIT template (Diedrichsen, 2006) ($P < 0.001$ uncorrected). Significant group comparisons are shown in **E** and **F** (SCA6 controls > SCA6; Friedreich's ataxia controls > Friedreich's ataxia; paired *t*-tests). Data are shown at a height threshold of $P < 0.001$ uncorrected; see Tables 1 and 2 for bootstrap-corrected cluster-size thresholds. Age and movement frequency were used as covariates of no interest. Positions of the coronal slices are indicated in a sagittal view of the SUIT template. *y* = SUIT coordinate; Roman numerals refer to: cerebellar lobules according to Schmahmann *et al.* (1999).

cortex in controls ($P < 0.001$, bootstrap-corrected cluster-size threshold) (Grodd *et al.*, 2001; Stefanescu *et al.*, 2013). As expected, activation was strongest on the right, i.e. ipsilateral to the movement. Hand-movement-related activation was less in all three patient groups compared to their matched control group (Fig. 4B–D). Remaining activations were most pronounced in the patients with SCA6 and least in the patients with Friedreich's ataxia. Whereas the general pattern of activation was comparable to the controls in patients with SCA6 and Friedreich's ataxia, with a focus on the right superior hand representation (lobules V/VI), it was different in the patients with SCA3. Although activation of right lobule V (and VIII) was observed in the SCA3 group, activation was most prominent in the posterior and inferior cerebellum (maximum in Crus I) on the left. Local maxima and cluster sizes are summarized in Table 1.

Comparing SCA6 patients with their matched control group showed significantly higher activations in controls with a focus in right lobules V and VI ($P < 0.001$, bootstrap-corrected cluster-size threshold, paired samples *t*-test; Fig. 4E and Table 2). Likewise, comparing patients with Friedreich's ataxia and their matched controls showed significantly higher activations in controls that were most prominent in lobules V and VI (Fig. 4F and Table 2). There was no significant difference comparing patients with SCA3 and matched controls, possibly because activation in individual patients with SCA3 were scattered across the entire cerebellum and showed very little overlap (data not shown).

Table 1 Functional MRI results in the cerebellar cortex in the three patient groups (SCA6, Friedreich's ataxia, SCA3) and controls

Group		Height threshold		Expected voxels/cluster	Group	Height threshold		Expected voxels/cluster	Group	Height threshold		Expected voxels/cluster	Group	Height threshold		Expected voxels/cluster
Controls (n = 12) Vol [mm^3]	Area	4.025 Vol [mm^3] per lob	t-value	147 x y z [mm]	SCA6 Vol [mm^3]	4.025 Vol [mm^3] per lob	t-value	118 x y z [mm]	FRDA Vol [mm^3]	4.025 Vol [mm^3] per lob	t-value	81 x y z [mm]	SCA3 Vol [mm^3]	4.297 Vol [mm^3] per lob	t-value	110 x y z [mm]
18 599	Right IV	753	8.38	5 −57 −14	4592	1160	8.06	8 −51 −13	661	–	–	–	686	[46]*	[4.97]	[15 −45 −18]
			6.94	11 −52 −20			6.81	11 −52 −20								
	Right V	4549	11.61	5 −65 −14		3007	8.12	14 −49 −14		201	4.68	25 −48 −26		534	6.62	26 −40 −31
			11.60	24 −51 −18			7.61	11 −51 −16			4.2	21 −52 −23			5.74	16 −47 −19
	Right VI	6128	12.88	23 −54 −24		409	5.23	23 −52 −19		460	6.17	28 −50 −28		[104]*	[5.29]	[30 −42 −27]
			10.05	6 −67 −14												
	Right VII	903	10.92	15 −68 −46		–	–	–		–	–	–		–	–	–
			7.54	8 −72 −51												
	Vermis VI	842	10.60	5 −67 −16	1428	–	–	–		–	–	–	133	–	–	–
	Right VIIIa	3080	16.53	14 −66 −49		722	5.74	15 −63 −55		–	–	–		–	–	–
	Right VIIIb	1120	11.22	13 −64 −49		706	6.57	23 −55 −51	[64]*	[64]	[5.88]	[25 −46 −58]		144	5.46	22 −56 −49
5372	Left Crus I	735	6.37	−36 −54 −31	–	–	–	–	–	–	–	–	792	792	14.63	−45 −70 −31
	Left Crus II	–	–	–		–	–	–							13.41	−49 −71 −29
										–	–	–	120	120	5.57	−20 −83 −43
	Left V	822	6.67	0 −67 −15		–	–	–		–	–	–		–	–	–
			4.95	−6 −62 −9												
	Left VI	4635	7.87	−30 −53 −31	374	374	5.45	−29 −55 −24		–	–	–		–	–	–
			7.78	−28 −65 −19	170	170	5.38	−29 −69 −22								
1979	Left VII	874	6.97	−19 −73 −53	–	–	–	–		–	–	–	1291	654	7.38	−3 −77 −47
			5.97	−17 −76 −51											6.52	−19 −71 −53
	Left VIIIa	1091	6.04	−18 −66 −49	352	352	5.98	−31 −48 −60		–	–	–		621	7.46	−22 −58 −46
			5.75	−22 −62 −48											6.68	−21 −58 −51
													156	156	8.73	−12 −41 −49

Age and movement frequency were used as covariates of no interest. For simplification, functional MRI data are shown in only one of the matched control groups (Friedreich's ataxia controls). Results of one-sample t-tests are shown at height thresholds of $P < 0.001$ uncorrected and bootstrap-corrected cluster-size thresholds (<k>). Vol [mm^3] = volume of the blood oxygenation level-dependent signal in a cluster; Vol [mm^3] per lob = volume of the blood oxygenation level-dependent signal in a cerebellar lobule (Diedrichsen *et al.*, 2009); t-value = peak value of the cluster; x, y, z [mm] in SUIT coordinates; *expected number of voxels / cluster not reached. FRDA = Friedreich's ataxia.

Table 2 Functional MRI results in the cerebellar cortex: significant group comparisons

Group		Height threshold		Expected voxels / cluster	Group		Height threshold		Expected voxels / cluster
SCA6 Controls > SCA6		3.485		144	FRDA Controls > FRDA		3.485		124
Vol [mm^3]	Vol [mm^3] per lob	Area	t-value	x y z [mm]	Vol [mm^3]	Vol [mm^3] per lob	Area	t-value	x y z [mm]
–	–	Right IV	–	–	[81]*	[81]	[Right IV]	[4.83]	[6 -56 -1]
549	359	Right V	4.29	2 −69 −9	404	120	Right V	3.95	21 −52 −25
1985	440	Right V	4.05	21 −54 −14		–	Right V	–	–
	1545	Right VI	4.88	26 −55 −27		284	Right VI	4.00	22 −52 −25
240	86	Right CrusII	4.54	3 −81 −33	–	–	Right CrusII	–	–
	123	Left CrusII	4.39	−1 −82 −33	–	–	Left CrusII	–	–
508	508	Left VI	4.47	−31 −60 −23	203	203	Left VI	4.57	−20 −59 −29
305	145	Left VII	4.39	−13 −71 −51	–	–	Left VII	–	–
	115	Left VIIIa	4.46	−13 −70 −51	323	40	Left VIIIa	3.98	−23 −56 −54
						280	Left VIIIb	4.28	−21 −52 −55

Age and movement frequency were used as covariates of no interest. Data of group comparisons that showed significant differences are shown: SCA6 controls > SCA6 and Friedreich's ataxia controls > Friedreich's ataxia. Results of two-sample *t*-tests are shown at height thresholds of $P < 0.001$ uncorrected and bootstrap-corrected cluster-size thresholds (<k>). Vol [mm^3] = volume of the blood-oxygenation-level-dependent signal in a cluster; Vol [mm^3] per lob = volume of the blood-oxygenation-level-dependent signal in a cerebellar lobule (Diedrichsen *et al.*, 2009); *t*-value = peak value of the cluster; *x, y, z* [mm] in SUIT coordinates; * = expected number of voxels / cluster not reached. FRDA = Friedreich's ataxia.

Correlation analysis between mean individual beta values in the cerebellar cortex (lobules IV–VIII) and total SARA scores, and between beta values and trinucleotide repeat length was performed in the three patient groups. No significant correlations were observed (all *P*-values > 0.05). The best correlation coefficients were observed in SCA3 patients comparing beta values in right lobule V and SARA score (R = −0.603, $P = 0.065$), and in Friedreich's ataxia patients comparing beta values and GAA-repeat lengths in lobule VIII on the right (right lobule VIII: R = 0.656, $P = 0.055$; left lobule VIII: R = 0.612, $P = 0.08$; Pearson's correlation coefficient, two-sided).

Dentate nuclei

Activation related to hand movements was found in dentate nuclei bilaterally in controls ($P < 0.01$, bootstrap-corrected cluster-size threshold; Fig. 5 and Table 3). Activation was strongest in the right dorsorostral dentate and extended into the dorsocaudal and ventral parts of the nuclei. Activation was less in the three patient groups. In the Friedreich's ataxia group, no significant activation was observed (Fig. 5C). In SCA6 patients, the pattern of activation was similar to controls with most pronounced activations in the dorsal parts ($P < 0.01$, bootstrap-corrected cluster-size threshold; Fig. 5B). The pattern of activation in SCA3 was different and most pronounced in the ventral parts of the dentate nuclei bilaterally (Fig. 5D).

Group comparisons showed significantly greater dentate activation in matched controls compared to patients with SCA6, and in matched controls compared to Friedreich's ataxia patients (Fig. 5E and F and Table 3) ($P < 0.01$, bootstrap-corrected cluster-size threshold, paired samples *t*-test). SCA3 patients showed significantly more activation in the ventral part of the dentate compared to matched controls (Fig. 5G).

Correlation analysis between mean individual beta values in the dentate nuclei and total SARA scores, and between beta values and trinucleotide repeat lengths was performed in the three patient groups. No significant correlations were observed (all *P*-values > 0.05). The largest Pearson's correlation coefficient was observed comparing beta values in left dentate and total SARA score in SCA6 patients (R = 0.541, $P = 0.070$).

Discussion

Structural and functional MRI abnormalities were observed in patients with SCA6, Friedreich's ataxia, and SCA3 on the level of the cerebellar cortex and cerebellar nuclei. As expected, volume of the cerebellum was most markedly reduced in SCA6, with no significant reduction in Friedreich's ataxia and a slight decrease in SCA3. Atrophy of the cerebellar nuclei, however, was not only present in Friedreich's ataxia and SCA3, but also in SCA6. In fact, volume reduction of the nuclei was most marked in SCA6. On a functional level, functional MRI signal was altered both within the cerebellar cortex and the nuclei in the three disorders. In the nuclei, the reduction was most prominent in Friedreich's ataxia. Different from initial expectations, the decrease of functional MRI signal in the cerebellar cortex appeared more prominent in SCA3 and Friedreich's ataxia than in SCA6. In the following, these findings will be discussed in further detail in the light of the known pathohistology of the diseases.

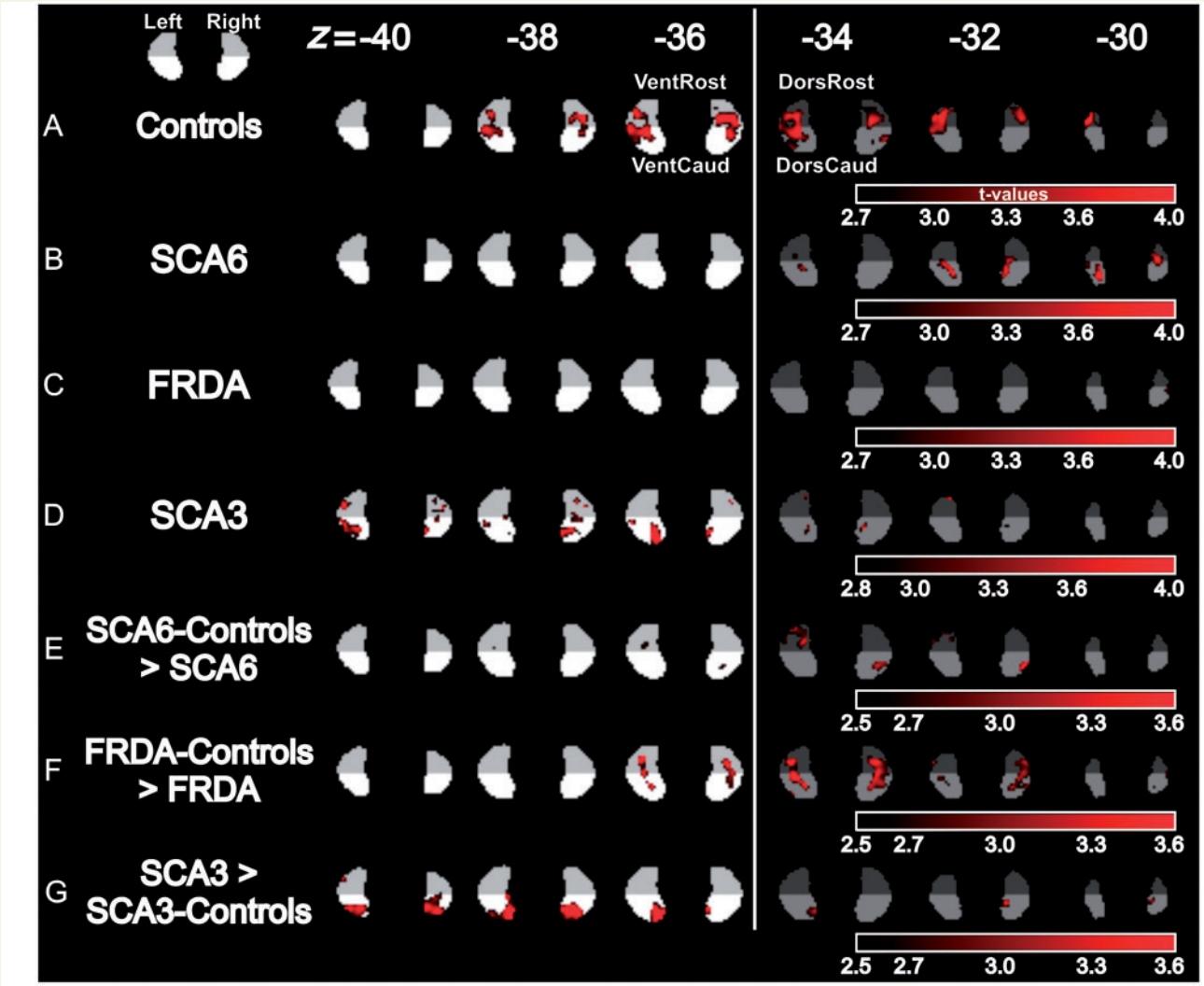

Figure 5 Functional MRI results in the dentate nuclei. Hand movement-related activations in one of the control groups (**A**, Friedreich's ataxia controls) and the three patient groups (**B**, SCA6; **C**, Friedreich's ataxia; **D**, SCA3) are mapped onto axial sections of the dentate template (Diedrichsen *et al.*, 2011). Significant group comparisons are shown in **E** (SCA6 controls > SCA6), **F** (Friedreich's ataxia controls > Friedreich's ataxia) and **G** (SCA3 > SCA3 controls; paired *t*-tests). Data are shown at a height threshold of $P < 0.01$ uncorrected; see Table 3 for bootstrap-corrected cluster-size thresholds. Age and movement frequency were used as covariates of no interest. Subdivisions of the dentate nuclei: DorsRost = dorsorostral; DorsCaud = dorsocaudal; VentRost = ventrorostral; VentCaud = ventrocaudal (according to Küper *et al.*, 2011). *z* = SUIT coordinate.

SCA6

Atrophy of the cerebellum is well known in SCA6 and, as expected, was confirmed in the present study (Lukas *et al.*, 2006; Schulz *et al.*, 2010). Cerebellar atrophy is caused by degeneration of the cerebellar cortex (Sasaki *et al.*, 1998; Yang *et al.*, 2000). The cerebellar nuclei have commonly been thought to be preserved in SCA6. In SWI images, however, marked atrophy of the cerebellar nuclei was observed both on the group and individual level. Reduced size of cerebellar nuclei has also been reported in a small group of SCA6 patients using diffusion tensor imaging (DTI; Du *et al.*, 2010). These findings support more recent histological data that show degeneration of the cerebellar nuclei in SCA6 (Wang *et al.*, 2010; Koeppen *et al.*, 2013; Rüb *et al.*, 2013).

Atrophy of the cerebellar nuclei has also been observed in the Lurcher mouse, which is a model of primary Purkinje cell degeneration. Heckroth (1994) reported a total nuclear volume reduction of 60%. Assuming similar pathogenesis in SCA6, degeneration of the cerebellar nuclei must be secondary to the Purkinje cell degeneration (Triarhou *et al.*, 1987; Linnemann *et al.*, 2004). In SCA3 and Friedreich's ataxia grumose degeneration of the Purkinje cell–nuclear cell synapse is followed by anterograde degeneration of cerebellar nuclei, but not by retrograde degeneration of the Purkinje cells (Koeppen, 2005; Koeppen and Mazurkiewicz, 2013). This difference may explain why nuclear atrophy appeared more pronounced in SCA6 than in Friedreich's ataxia and SCA3. Later age of onset in SCA6 may further contribute. Disease duration cannot explain

Table 3 Functional MRI results in the cerebellar nuclei in the three patient groups (SCA6, Friedreich's ataxia, SCA3) and controls

Controls (n = 12)					SCA6			FRDA			SCA3		
	<k> = 89			T = 2.718	<k> = 102		T = 2.718	<k> = 74		T = 2.718	<k> = 100		T = 2.821
	Side	Vol [mm^3]	t-value	x y z [mm]	Vol [mm^3]	t-value	x y z [mm]	Vol [mm^3]	t-value	x y z [mm]	Vol [mm^3]	t-value	x y z [mm]
Dentate	Right	395	6.39 4.92	20 −54 −37 16 −54 −36	97	4.30 4.00	11 −61 −32 13 −56 −31	–	– –	– –	180	4.79 3.94	11 −63 −38 19 −52 −37
	Left	673	5.82 4.76	−14 −55 −30 −18 −52 −37	112	6.52 2.85	−10 −63 −30 −16 −55 −35	–	– –	– –	90 111	5.64 4.90	−11 −65 −36 −14 −62 −41

SCA6 Controls > SCA6					FRDA Controls > FRDA			SCA3 > SCA3 Controls		
	<k> = 88			T = 2.500	<k> = 88		T = 2.500	<k> = 106		T = 2.539
	Side	Vol [mm^3]	t-value	x y z [mm]	Vol [mm^3]	t-value	x y z [mm]	Vol [mm^3]	t-value	x y z [mm]
Dentate	Right	[57]*	[4.19]	[18 −64 −32]	350	4.39 3.31	18 −53 −36 19 −62 −33	255	5.61	15 −63 −38
	Left	130	3.82 3.03	−11 −53 −33 −19 −54 −33	180	5.80	−15 −59 −34	347	5.60 3.54	−11 −64 −37 −19 −51 −41

Age and movement frequency were used as covariates of no interest. For simplification, functional MRI data are shown in only one of the matched control groups (Friedreich's ataxia controls). Results of one-sample *t*-tests are shown in the upper rows and results of two-sample *t*-tests in the lower rows. Only results of group comparisons that were significant are shown (SCA6 controls > SCA6; Friedreich's ataxia controls > Friedreich's ataxia; SCA3 > SCA3 controls). Results are shown at height thresholds of $P < 0.01$ uncorrected (T) and bootstrap-corrected cluster-size thresholds (<k>). Vol [mm^3] = volume of the blood-oxygenation-level-dependent signal in the dentate nucleus. *t*-value = peak value of the cluster; *x*, *y*, *z* [mm] in SUIT coordinates; * = expected number of voxels / cluster not reached. FRDA = Friedreich's ataxia.

the difference, as it was significantly longer in Friedreich's ataxia compared to SCA6 patients, but similar between SCA6 and SCA3 patients. Comparative post-mortem studies are needed for clarification.

As expected, functional MRI revealed a significant decrease of hand movement-related activation at the level of the cerebellar cortex. It should be noted, however, that decreased functional MRI signal is unlikely a direct reflection of the reduced number of Purkinje cells. Recent studies investigating the underlying physiology of functional MRI signals revealed that synaptic input of climbing and mossy fibres as well as inhibitory interneurons increase functional MRI signals in the cerebellar cortex, but not the spiking rate of the Purkinje cells (Lauritzen *et al.*, 2012). Interneurons, climbing fibres, and parallel fibres seem to be preserved in the molecular layer in SCA6 (Koeppen, 2005). A reduced number of synaptic Purkinje cell dendritic targets likely explains reduced functional MRI signal. Different from initial expectations, there was no compensatory increase of functional MRI signal within the cerebellar nuclei. Rather, functional MRI signal was significantly reduced in SCA6 patients compared to control subjects. As yet, the physiology of functional MRI signal in the cerebellar nuclei has not been studied. Excitatory collaterals of mossy and climbing fibre afferent input may play a role. Again, reduction of synaptic nuclear cell targets may explain the decreased functional MRI signal. Because inhibitory synpases may also increase functional MRI signal, reduced Purkinje cell afferents are another possible cause.

Friedreich's ataxia

As expected and in confirmation of findings in the literature, we did not observe a significant reduction of cerebellar volume in Friedreich's ataxia (Ormerod *et al.*, 1994). Cerebellar atrophy can occur in Friedreich's ataxia, but this is an uncommon finding. In addition, a significant size reduction of the cerebellar nuclei was observed. Degeneration of the cerebellar nuclei is well known based on histological studies (Koeppen and Mazurkiewicz, 2013), and volume reduction in SWI images has already been shown in another study by our group (Solbach *et al.*, 2014).

Disordered iron metabolism is known to play a role in Friedreich's ataxia. Because iron content is already high in the healthy dentate nuclei, cerebellar nuclei may be susceptible for the disease. Iron accumulates in the mitochondria (Richardson *et al.*, 2010). Possible impact on the appearance of dentate nuclei on SWI images, however, is likely limited. Koeppen and coworkers have performed the most detailed post-mortem analyses of the dentate nuclei in Friedreich's ataxia (Koeppen *et al.*, 2007; Koeppen and Mazurkiewicz, 2013). In contrast to neurodegeneration with brain iron accumulation (NBIA) there is no overall accumulation of iron in the cerebellar nuclei. The dentate nuclei, however, are smaller in Friedreich's ataxia compared to healthy controls. Furthermore, total iron and ferritin concentrations (micromol per gram wet weight) in the dentate nuclei have been shown to be the same in Friedreich's ataxia as in healthy controls (Koeppen *et al.*, 2007). There is known mitochondrial iron overload in the

Purkinje cell–dentate neuron synapse. Mitochondrial iron dysmetabolism is thought to be the cause of grumose degeneration of the Purkinje cell–dentate neuron synapse, which is followed by consecutive loss of neurons within the dentate nucleus. Notably iron distribution shifts at the cellular level, but, as stated above, there is no change in the total iron content. This shift of iron distribution at the cellular level is unlikely to be detected with the spatial resolution of SWI images. Furthermore, because there seems to be no total increase of iron in the dentate nuclei, it appears less likely that iron dysmetabolism is a major confound of reduced functional MRI signal.

Note that previous magnetic resonance relaxometry studies seem to be at variance with histological data of normal total iron content (Waldvogel *et al.*, 1999; Boddaert *et al.*, 2007; Bonilha da Silva *et al.*, 2014; see also Synofzik *et al.*, 2011 using transcranial sonography). Abnormal magnetic resonance relaxometry (that is, reduced relaxation time) has been interpreted as indication of increased iron content in dentate nuclei in Friedreich's ataxia. In a recent study of our own group, however, we were unable to replicate these findings (Solbach *et al.*, 2014). We found smaller nuclei volumes, but no change in magnetic resonance relaxometry measures. Our region of interest was carefully placed within the cerebellar nuclei (based on SWI images) and did not include surrounding white matter. Because magnetic resonance relaxometry is not a specific indicator of iron levels, especially if abnormal tissue is involved, other factors such as abnormal tissue density, myelin content, and water content may have contributed to previous findings. Assessment of atrophy of the cerebellar nuclei based on SWI images appears to be a more robust measure of nuclear disease in Friedreich's ataxia.

Volume reduction of the cerebellar nuclei was accompanied by decreased functional MRI signal. Furthermore, although there was no cerebellar volume reduction in Friedreich's ataxia, functional MRI signal in the cerebellar cortex was significantly reduced. Decline of functional MRI signal in the cerebellar cortex has also been observed in Friedreich's ataxia by others (Akhlaghi *et al.*, 2012; Ginestroni *et al.*, 2012). Thus, although neither structural MRI nor histology show morphological changes within the cerebellar cortex, functional MRI signal is reduced. Reduced functional MRI signal may be caused, at least in part, by the known degeneration of spinocerebellar tracts in Friedreich's ataxia. As outlined above, it is the synpases between climbing fibres, mossy fibres, and interneurons with the Purkinje cells that underly the functional MRI signal. Inferior olive and climbing fibres are preserved in Friedreich's ataxia (Koeppen *et al.*, 2013). In the current study, patients had to perform a simple hand movement, and the spinocerebellum appears to be most important. Given that spinocerebellar tracts degenerate in Friedreich's ataxia, we postulate that mossy fibre input to the spinocerebellum is reduced and results in reduced functional MRI signal. As yet, however, the density of mossy fibres projecting to the spinocerebellum has never been systematically assessed. Lack of functional MRI signal in the nuclei is likely explained by the grumose degeneration of the Purkinje cell–nuclear cell synapse (Koeppen *et al.*, 2007; Koeppen and Mazurkiewicz, 2013), which also hampers the mossy fibre and climbing fibre collaterals to the nuclear cells (Arnulf Koeppen, personal communication).

SCA3

Similar to SCA6 and Friedreich's ataxia, volume reduction of the cerebellum in SCA3 matched well with findings of the literature and showed a mild reduction (Bürk *et al.*, 1996; Klockgether *et al.*, 1998; Reetz *et al.*, 2013). In addition, SWI revealed atrophy of the cerebellar nuclei in SCA3. Findings are in good accordance with histological data that show substantial atrophy of cerebellar nuclei in SCA3 (Koeppen *et al.*, 2013).

Similar to Friedreich's ataxia, functional MRI signal of the cerebellar cortex was reduced although this did not reach significance. Reasons for reduced functional MRI signal may be the same: similar to Friedreich's ataxia there is known degeneration of spinocerebellar tracts (Dürr *et al.*, 1996; Koeppen *et al.*, 2013). Whereas some authors report no abnormalities of the cerebellar cortex (Koeppen et *al.*, 2013), others observed grey matter reduction (Scherzed *et al.*, 2012; Reetz *et al.*, 2013). Therefore, a reduced number of synaptic Purkinje cell dendritic targets may also contribute. The pattern of remaining activation was different in SCA3 compared to Friedreich's ataxia and SCA6. Whereas in Friedreich's ataxia and SCA6 activation was most prominent in the known hand areas within the cerebellar cortex and nuclei, more posterolateral areas of the cerebellar hemisphere and more ventral areas of the dentate nuclei were activated in SCA3. Activation in the ventral dentate nucleus was significantly higher in SCA3 patients compared to controls. These areas are pontocerebellar (Glickstein and Doron, 2008). There are histological data showing that pontine mossy fibre afferences are preserved in SCA3 (Koeppen *et al.*, 2013). SCA3 patients may activate pontocerebellar areas to compensate for dysfunction of the spinocerebellum. Likewise, premotor cortex and neighbouring Brodmann area 44 showed additional activations in SCA3 patients compared to controls, although group difference did not reach significance. Brodmann area 44 is known to partly overlap and interact with premotor cortex (Binkofski and Buccino, 2004). Cerebellar cortical activations in SCA3 patients were most prominent in Crus I which has known connections with premotor cortex (Hashimoto *et al.*, 2010).

General discussion

It should be emphasized that cerebellar nuclei volumes assessed on the SWI images do not reflect the actual volumes. Firstly, at the present state it is unclear to what extent volumes of the dentate nuclei may be confounded by possible disease-related changes in iron deposition. Because

high iron content reduces functional MRI signal the same limitation may apply to functional MRI data of the nuclei. The content and distribution of iron has never been assessed in the dentate nuclei in SCA3 and SCA6. As yet, however, there is no indication that disordered iron metabolism plays a central role in the pathogenesis of SCA3 and SCA6 (Orr, 2012; Evers *et al.*, 2014). Furthermore, the known changes in iron metabolism in Friedreich's ataxia are unlikely to affect appearance of the nuclei on SWI images because total iron content is not different from controls (see also more detailed discussion above).

Secondly, as outlined in the 'Materials and methods' section, the extent of the cerebellar nuclei is artificially increased in SWI phase images. It should be noted that in previous studies by our group, phase images were used to calculate dentate nuclei volume (Diedrichsen *et al.*, 2011; Solbach *et al.*, 2014). This led to abnormally large volumes in control subjects (mean volume of individual dentate nucleus: 364.4 SD 87.2 mm^3; see Table 1 in Diedrichsen *et al.*, 2011). In the present study, calculations were based on SWI images and were corrected on magnitude images. Volumes were closer to volumes given in the histological literature (present study: 200.1 SD 89.3 mm^3; Höpker, 1951: 155 mm^3). However, even at a field strength of 7 T and an isotropic voxel size of 0.5 mm, resolution of the cerebellar nuclei is still below histology. Quantitative magnetic susceptibility mapping (QSM) is a further development of SWI. QSM allows for much improved anatomical delineation of deep grey matter structures (Deistung *et al.*, 2013) and for accurate quantification of iron content (Langkammer *et al.*, 2012). Its future application will likely further improve imaging of the cerebellar nuclei in both healthy and diseased subjects.

The present study was performed using a 7 T MRI scanner. Studies in healthy subjects show that the cerebellar nuclei can also be visualized using more common field strengths (1.5 T and 3 T; Maderwald *et al.*, 2012). Thus, atrophy of the cerebellar nuclei in hereditary ataxias is likely to be observed as well using 1.5 T and 3 T MRI, but this needs to be confirmed in future studies.

Conclusion

The present data show that SWI imaging is useful to depict pathology of the cerebellar nuclei in hereditary ataxias. Atrophy of the cerebellar nuclei was present in SCA6, Friedreich's ataxia, and SCA3. Functional MRI showed that there is general dysfunction of the cerebellum in SCA6, Friedreich's ataxia, and SCA3 that is not limited to the cerebellar cortex in SCA6 or the cerebellar nuclei in Friedreich's ataxia and SCA3. It will be of interest to use structural and functional MRI to study the cerebellar nuclei in other hereditary ataxias in the future. Furthermore, long-term studies would be of interest to determine whether quantification of nuclear pathology is a useful biomarker of disease progression and response to therapeutic interventions.

Acknowledgements

The authors would like to thank Fahad Sultan and Arnulf Koeppen for most helpful discussions.

Funding

The study was supported by the EU Marie Curie Initial Training Network (ITN) grant C7 ('Cerebellar-Cortical Control: Cells, Circuits, Computation, and Clinic').

Supplementary material

Supplementary material is available at *Brain* online.

References

Akhlaghi H, Corben L, Georgiou-Karistianis N, Bradshaw J, Delatycki MB, Storey E, et al. A functional MRI study of motor dysfunction in Friedreich's ataxia. Brain Res 2012; 1471: 138–54.

Ashburner J. A fast diffeomorphic image registration algorithm. Neuroimage 2007; 38: 95–113.

Ashburner J. Computational anatomy with the SPM software. Magn Reson Imaging 2009; 27: 1163–74.

Binkofski F, Buccino G. Motor functions of the Broca's region. Brain Lang 2004; 89: 362–9.

Boddaert N, Le Quan Sang KH, Rötig A, Leroy-Willig A, Gallet S, Brunelle F, et al. Selective iron chelation in Friedreich ataxia: biologic and clinical implications. Blood 2007; 110: 401–8.

Bonilha da Silva C, Bergo FP, D'Abreu A, Cendes F, Lopes-Cendes I, França MC Jr. Dentate nuclei T2 relaxometry is a reliable neuroimaging marker in Friedreich's ataxia. Eur J Neurol 2014; 21: 1131–6.

Brandauer B, Hermsdörfer J, Beck A, Aurich V, Gizewski ER, Marquardt C, et al. Impairments of prehension kinematics and grasping forces in patients with cerebellar degeneration and the relationship to cerebellar atrophy. Clin Neurophysiol 2008; 119: 2528–37.

Bürk K, Abele M, Fetter M, Dichgans J, Skalej M, Laccone F, et al. Autosomal dominant cerebellar ataxia type I clinical features and MRI in families with SCA1, SCA2 and SCA3. Brain 1996; 119: 1497–505.

Deistung A, Schäfer A, Schweser F, Biedermann U, Turner R, Reichenbach JR. Toward *in vivo* histology: a comparison of quantitative susceptibility mapping (QSM) with magnitude-, phase-, and R2*-imaging at ultra-high magnetic field strength. Neuroimage 2013; 65: 299–314.

Diedrichsen J. A spatially unbiased atlas template of the human cerebellum. Neuroimage 2006; 33: 127–38.

Diedrichsen J, Balsters JH, Flavell J, Cussans E, Ramnani N. A probabilistic MR atlas of the human cerebellum. Neuroimage 2009; 46: 39–46.

Diedrichsen J, Maderwald S, Küper M, Thürling M, Rabe K, Gizewski ER, et al. Imaging the deep cerebellar nuclei: a probabilistic atlas and normalization procedure. Neuroimage 2011; 54: 1786–94.

Du AX, Cuzzocreo JL, Landman BA, Zee DS, Prince JL, Ying SH. Diffusion tensor imaging reveals disease-specific deep cerebellar nuclear changes in cerebellar degeneration. J Neurol 2010; 257: 1406–8.

Dürr A, Stevanin G, Cancel G, Duyckaerts C, Abbas N, Didierjean O, et al. Spinocerebellar ataxia 3 and Machado-Joseph disease: clinical,

molecular, and neuropathological features. Ann Neurol 1996; 39: 490–9.
Dürr A. Autosomal dominant cerebellar ataxias: polyglutamine expansions and beyond. Lancet Neurol 2010; 9: 885–94.
Eickhoff SB, Stephan KE, Mohlberg H, Grefkes C, Fink GR, Amunts K, et al. A new SPM toolbox for combining probabilistic cytoarchitectonic maps and functional imaging data. Neuroimage 2005; 25: 1325–35.
Evers MM, Toonen LJ, van Roon-Mom WM. Ataxin-3 protein and RNA toxicity in spinocerebellar ataxia type 3: current insights and emerging therapeutic strategies. Mol Neurobiol 2014; 49: 1513–31.
Friston KJ, Frith CD, Turner R, Frackowiak RS. Characterizing evoked hemodynamics with fMRI. Neuroimage 1995; 2: 157–65.
Gasparotti R, Pinelli L, Liserre R. New MR sequences in daily practice: susceptibility weighted imaging. A pictorial essay. Insights Imaging 2011; 2: 335–47.
Geyer S, Ledberg A, Schleicher A, Kinomura S, Schormann T, Bürgel U, et al. Two different areas within the primary motor cortex of man. Nature 1996; 382: 805–7.
Gierga K, Schelhaas HJ, Brunt ER, Seidel K, Scherzed W, Egensperger R, et al. Spinocerebellar ataxia type 6 (SCA6): neurodegeneration goes beyond the known brain predilection sites. Neuropathol Appl Neurobiol 2009; 35: 515–27.
Ginestroni A, Diciotti S, Cecchi P, Pesaresi I, Tessa C, Giannelli M, et al. Neurodegeneration in Friedreich's ataxia is associated with a mixed activation pattern of the brain. A fMRI study. Hum Brain Mapp 2012; 33: 1780–91.
Glickstein M, Doron K. Cerebellum: connections and functions. Cerebellum 2008; 7: 589–94.
Glover GH, Li TQ, Ress D. Image-based method for retrospective correction of physiological motion effects in fMRI: RETROICOR. Magn Reson Med 2000; 44: 162–7.
Grodd W, Hülsmann E, Lotze M, Wildgruber D, Erb M. Sensorimotor mapping of the human cerebellum: fMRI evidence of somatotopic organization. Hum Brain Mapp 2001; 13: 55–73.
Habas C. Functional imaging of the deep cerebellar nuclei: a review. Cerebellum 2010; 9: 22–8.
Hashimoto M, Takahara D, Hirata Y, Inoue K, Miyachi S, Nambu A, Tanji J, Takada M, Hoshi E. Motor and non-motor projections from the cerebellum to rostrocaudally distinct sectors of the dorsal premotor cortex in macaques. Eur J Neurosci 2010; 31: 1402–13.
Hayasaka S, Nichols TE. Validating cluster size inference: random field and permutation methods. Neuroimage 2003; 20: 2343–56.
Heckroth JA. A quantitative morphological analysis of the cerebellar nuclei in normal and lurcher mutant mice. II. Volumetric changes in cytological components. J Comp Neurol 1994; 343: 183–92.
Höpker W. Das Altern des Nucleus dentatus. Z. Altersforschung 1951; 5: 256–77.
Klockgether T. Update on degenerative ataxias. Curr Opin Neurol 2011; 24: 339–45.
Klockgether T, Petersen D, Grodd W, Dichgans J. Early onset cerebellar ataxia with retained tendon reflexes. Clinical, electrophysiological and MRI observations in comparison with Friedreich's ataxia. Brain 1991; 114: 1559–73.
Klockgether T, Skalej M, Wedekind D, Luft AR, Welte D, Schulz JB, et al. Autosomal dominant cerebellar ataxia type I. MRI-based volumetry of posterior fossa structures and basal ganglia in spinocerebellar ataxia types 1, 2 and 3. Brain 1998; 121: 1687–93.
Koeppen AH. The pathogenesis of spinocerebellar ataxia. Cerebellum 2005; 4: 62–73.
Koeppen AH, Mazurkiewicz JE. Friedreich ataxia: neuropathology revised. J Neuropathol Exp Neurol 2013; 72: 78–90.
Koeppen AH, Michael SC, Knutson MD, Haile DJ, Qian J, Levi S, et al. The dentate nucleus in Friedreich's ataxia: the role of iron-responsive proteins. Acta Neuropathol 2007; 114: 163–73.
Koeppen AH, Ramirez RL, Bjork ST, Bauer P, Feustel PJ. The reciprocal cerebellar circuitry in human hereditary ataxia. Cerebellum 2013; 12: 493–503.
Küper M, Dimitrova A, Thürling M, Maderwald S, Roths J, Elles HG, et al. Evidence for a motor and a non-motor domain in the human dentate nucleus–an fMRI study. Neuroimage 2011; 54: 2612–22.
Küper M, Thürling M, Stefanescu R, Maderwald S, Roths J, Elles HG, et al. Evidence for a motor somatotopy in the cerebellar dentate nucleus—an FMRI study in humans. Hum Brain Mapp 2012; 33: 2741–9.
Langkammer C, Schweser F, Krebs N, Deistung A, Goessler W, Scheurer E, et al. Quantitative susceptibility mapping (QSM) as a means to measure brain iron? A post mortem validation study. Neuroimage 2012; 62: 1593–9.
Lauritzen M, Mathiesen C, Schaefer K, Thomsen KJ. Neuronal inhibition and excitation, and the dichotomic control of brain hemodynamic and oxygen responses. Neuroimage 2012; 62: 1040–50.
Linnemann C, Sultan F, Pedroarena CM, Schwarz C, Thier P. Lurcher mice exhibit potentiation of GABA(A)-receptor-mediated conductance in cerebellar nuclei neurons in close temporal relationship to Purkinje cell death. J Neurophysiol 2004; 91: 1102–7.
Lukas C, Schöls L, Bellenberg B, Rüb U, Przuntek H, Schmid G, et al. Dissociation of grey and white matter reduction in spinocerebellar ataxia type 3 and 6: a voxel-based morphometry study. Neurosci Lett 2006; 408: 230–5.
Maderwald S, Thürling M, Küper M, Theysohn N, Müller O, Beck A, et al. Direct visualization of cerebellar nuclei in patients with focal cerebellar lesions and its application for lesion-symptom mapping. Neuroimage 2012; 63: 1421–31.
Marques JP, Gruetter R, van der Zwaag W. *In vivo* structural imaging of the cerebellum, the contribution of ultra-high fields. Cerebellum 2012; 11: 384–91.
Oldfield RC. The assessment and analysis of handedness: the Edinburgh inventory. Neuropsychologia 1971; 9: 97–113.
Ormerod IE, Harding AE, Miller DH, Johnson G, MacManus D, du Boulay EP, et al. Magnetic resonance imaging in degenerative ataxic disorders. J Neurol Neurosurg Psychiatry 1994; 57: 51–57.
Orr HT. Cell biology of spinocerebellar ataxia. J Cell Biol 2012; 197: 167–77.
Poser BA, Norris DG. Investigating the benefits of multi-echo EPI for fMRI at 7 T. Neuroimage 2009; 45: 1162–72.
Reetz K, Costa AS, Mirzazade S, Lehmann A, Juzek A, Rakowicz M, et al. Genotype-specific patterns of atrophy progression are more sensitive than clinical decline in SCA1, SCA3 and SCA6. Brain 2013; 136: 905–17.
Richardson DR, Huang ML, Whitnall M, Becker EM, Ponka P, Suryo Rahmanto Y. The ins and outs of mitochondrial iron-loading: the metabolic defect in Friedreich's ataxia. J Mol Med (Berl) 2010; 88: 323–9.
Rüb U, Schöls L, Paulson H, Auburger G, Kermer P, Jen JC, et al. Clinical features, neurogenetics and neuropathology of the polyglutamine spinocerebellar ataxias type 1, 2, 3, 6 and 7. Prog Neurobiol 2013; 104: 38–66.
Sasaki H, Kojima H, Yabe I, Tashiro K, Hamada T, Sawa H, et al. Neuropathological and molecular studies of spinocerebellar ataxia type 6 (SCA6). Acta Neuropathol 1998; 95: 199–204.
Scherzed W, Brunt ER, Heinsen H, de Vos RA, Seidel K, Bürk K, et al. Pathoanatomy of cerebellar degeneration in spinocerebellar ataxia type 2 (SCA2) and type 3 (SCA3). Cerebellum 2012; 11: 749–60.
Schmitz-Hübsch T, du Montcel ST, Baliko L, Berciano J, Boesch S, Depondt C, et al. Scale for the assessment and rating of ataxia: development of a new clinical scale. Neurology 2006; 66: 1717–20.
Schulz JB, Boesch S, Bürk K, Dürr A, Giunti P, Mariotti C, et al. Diagnosis and treatment of Friedreich ataxia: a European perspective. Nat Rev Neurol 2009; 5: 222–34.
Schulz JB, Borkert J, Wolf S, Schmitz-Hübsch T, Rakowicz M, Mariotti C, et al. Visualization, quantification and correlation of brain atrophy with clinical symptoms in spinocerebellar ataxia types 1, 3 and 6. Neuroimage 2010; 49: 158–68.

Schmahmann JD, Doyon J, McDonald D, Holmes C, Lavoie K, Hurwitz AS, et al. Three-dimensional MRI atlas of the human cerebellum in proportional stereotaxic space. Neuroimage 1999; 10: 233–60.

Seidel K, Siswanto S, Brunt ER, den Dunnen W, Korf HW, Rüb U. Brain pathology of spinocerebellar ataxias. Acta Neuropathol 2012; 124: 1–21.

Solbach K, Kraff O, Minnerop M, Beck A, Schöls L, Ladd M, et al. Cerebellar pathology in Friedreich's ataxia: atrophied nuclei with normal iron content. Neuroimage Clin 2014; 6: 93–9.

Stefanescu MR, Thürling M, Maderwald S, Wiestler T, Ladd ME, Diedrichsen J, et al. A 7T fMRI study of cerebellar activation in sequential finger movement tasks. Exp Brain Res 2013; 228: 243–54.

Synofzik M, Godau J, Lindig T, Schöls L, Berg D. Transcranial sonography reveals cerebellar, nigral, and forebrain abnormalities in Friedreich's ataxia. Neurodegener Dis 2011; 8: 470–5.

Theysohn JM, Maderwald S, Kraff O, Moenninghoff C, Ladd ME, Ladd SC. Subjective acceptance of 7 Tesla MRI for human imaging. MAGMA 2008; 21: 63–72.

Thürling M, Küper M, Stefanescu R, Maderwald S, Gizewski ER, Ladd ME, et al. Activation of the dentate nucleus in a verb generation task: A 7T MRI study. Neuroimage 2011; 57: 1184–91.

Triarhou LC, Norton J, Ghetti B. Anterograde transsynaptic degeneration in the deep cerebellar nuclei of Purkinje cell degeneration (pcd) mutant mice. Exp Brain Res 1987; 66: 577–88.

van de Warrenburg BP, van Gaalen J, Boesch S, Burgunder JM, Dürr A, Giunti P, et al. EFNS/ENS Consensus on the diagnosis and management of chronic ataxias in adulthood. Eur J Neurol 2014; 21: 552–62.

Verstynen TD, Deshpande V. Using pulse oximetry to account for high and low frequency physiological artifacts in the BOLD signal. Neuroimage 2011; 55: 1633–44.

Waldvogel D, van Gelderen P, Hallett M. Increased iron in the dentate nucleus of patients with Friedrich's ataxia. Ann Neurol 1999; 46: 123–5.

Wang X, Wang H, Xia Y, Jiang H, Shen L, Wang S, et al. A neuropathological study at autopsy of early onset spinocerebellar ataxia 6. J Clin Neurosci 2010; 17: 751–5.

Weier K, Beck A, Magon S, Amann M, Naegelin Y, Penner IK, et al. Evaluation of a new approach for semi-automatic segmentation of the cerebellum in patients with multiple sclerosis. J Neurol 2012; 259: 2673–80.

Yang Q, Hashizume Y, Yoshida M, Wang Y, Goto Y, Mitsuma N, et al. Morphological Purkinje cell changes in spinocerebellar ataxia type 6. Acta Neuropathol 2000; 100: 371–6.